Aalborg Universitet

AALBORG UNIVERSITY
DENMARK

Grid Inertial Response with Lithium-ion Battery Energy Storage Systems

Knap, Vaclav; Sinha, Rakesh; Swierczynski, Maciej Jozef; Stroe, Daniel Ioan; Chaudhary, Sanjay

Published in:
Proceedings of the 23rd IEEE International Symposium on Industrial Electronics, ISIE 2014

DOI (link to publication from Publisher):
10.1109/ISIE.2014.6864891

Publication date:
2014

Document Version
Accepted author manuscript, peer reviewed version

Link to publication from Aalborg University

Citation for published version (APA):
Knap, V., Sinha, R., Swierczynski, M. J., Stroe, D. I., & Chaudhary, S. (2014). Grid Inertial Response with Lithium-ion Battery Energy Storage Systems. In *Proceedings of the 23rd IEEE International Symposium on Industrial Electronics, ISIE 2014* (pp. 1817-1822). IEEE Press. https://doi.org/10.1109/ISIE.2014.6864891

General rights
Copyright and moral rights for the publications made accessible in the public portal are retained by the authors and/or other copyright owners and it is a condition of accessing publications that users recognise and abide by the legal requirements associated with these rights.

- Users may download and print one copy of any publication from the public portal for the purpose of private study or research.
- You may not further distribute the material or use it for any profit-making activity or commercial gain
- You may freely distribute the URL identifying the publication in the public portal -

Take down policy
If you believe that this document breaches copyright please contact us at vbn@aub.aau.dk providing details, and we will remove access to the work immediately and investigate your claim.

Downloaded from vbn.aau.dk on: March 28, 2024

Grid Inertial Response with Lithium-ion Battery Energy Storage Systems

Vaclav Knap, Rakesh Sinha, Maciej Swierczynski, Daniel-Ioan Stroe and Sanjay Chaudhary
Department of Energy Technology, Aalborg University, Denmark
Email: vkn@et.aau.dk

***Abstract*—The increased grid-penetration levels of energy produced by renewable sources, which have almost no inertia, might have a negative impact on the reliable and stable operation of the power system. Various solutions for mitigating the aforementioned problem were proposed in the literature. The aim of this paper is to evaluate the technical viability of utilizing energy storage systems based on Lithium-ion batteries for providing inertial response in grids with high penetration levels of wind power. In order to perform this evaluation, the 12-bus system grid model was used; the inertia of the grid was varied by decreasing the number of conventional power plants in the studied grid model while in the same time increasing the load and the wind power penetration levels. Moreover, in order to perform a realistic investigation, a dynamic model of the Lithium-ion battery was considered and parameterized. All the studies were performed in real time on a laboratory setup composed of RTDS and dSPACE platforms.**

I. Introduction

The current trend in energy generation is heading towards increasing renewable energy sources (RESs), mainly in form of wind and photovoltaics (PVs). European Union plans to achieve 20 % energy production and over 10 % share in transport covered by RES in 2020 [1]. Denmark plan towards 2020 is to possess over 35 % of energy production provided by RES and wind power is supposed to supply nearly half of the total electricity consumption [2].

Growing participation of RES in power systems leads to the replacement of thermal power plants, which further implies decreasing numbers of conventional power plants (CPPs) based on synchronous generators [3]. The typical attribute of CPPs is a direct coupling between the grid electrical frequency and speed of the generator rotor. Thus, the generator rotating mass behaves as a kinetic energy storage and provides inertial response (IR). Modern wind power plants (WPPs) are commonly equipped with power electronic interfaces, which decouple the generator speed from the grid frequency. Therefore, the IR of RES is not as inherent as it is in the case of CPPs [4]. As the reduced system inertia can affect the grid stability, there is a need for supplementing it. Different methods for emulating IR, such as using energy storage systems, curtailing RES, overloading WPP and demand side management are introduced in [4]. Moreover, VSC-HVDC systems represent an alternative solution to emulate the inertia of synchronous generators, as presented in [5]. Candidates for control of wind power plant IR are summarized in [6]. Inertial and frequency response from wind turbines, together with experimental tests, are presented in [7]. As a part of demand side management, multi-stage underfrequency load shedding is proposed in [8]. The utilisation of energy storage systems (ESSs) for IR is described in [9] and [10]. Studies for utilisation of the ESS based on ultracapacitors [10], [11], pumped hydros [12], [13], flywheels [14] and battery systems as Lead-Acid [15] and Sodium-Sulfur [16] for the IR have been carried out.

Another available energy storage technology are Lithium-ion (Li-ion) batteries, which are characterized by high efficiency, fast response and long life time [17]. This attributes makes them suitable for delivering grid services for short and medium time frame, like primary frequency reserve (PFR) [18]. PFR requirements does not demand the fully utilization of an unit directly after its activation. This time window can lead to further utilization of Li-ion based ESSs due to their fast response. Therefore, the focus of this paper is to evaluate the technical viability of utilizing the ESS based on Li-ion batteries for providing IR. Due to the short duration of the IR, the dynamics and limitations of the Li-ion battery have been considered using the standard detailed model of Li-ion battery provided by [19], [20].

Study cases are performed on the 12-bus grid model, which is modified to include WPPs and ESS. The laboratory setup consists of real time simulation platforms RTDS and dSPACE. They are appropriate for this investigation due to their computation performance for short term simulation.

The present paper is organized as follows: Section II describes the role and meaning of the IR in the grid. Section III presents modeling of the system and the simulation environment for studies. Two study cases together with operational metrics are included in Section IV. Conclusion is provided in Section V.

II. System inertia and frequency characteristics

Power system stability is defined as *"the ability of an electric power system, for a given initial operating condition, to regain a state of operating equilibrium after being subjected to a physical disturbance, with most system variables bounded so that practically the entire system remains intact"* [21]. In relation to large disturbances in active power balance, rotor angle and frequency stability are the main concern. While rotor angle stability is concerned with maintaining the system synchronism, frequency stability ensures the operation of the system in a tolerable point of frequency equilibrium with minimal loss of load. With frequency deviation over the limits, typically between 0.1 Hz/s and 1 Hz/s [22], protective relays

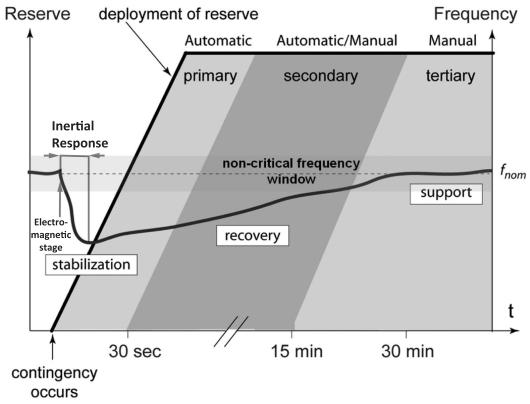


Fig. 1. Stages of frequency response by Union for the Co-ordination of Transmission of Electricity (UCTE) [26].

get activated and lead to island mode operation or up to the blackout of the system [21], [23].

In general, the response against sudden change in the active power balance is usually divided into five stages as it is shown in Fig. 1. The first stage is the electromagnetic energy release from the magnetic field of synchronous generator lasting approximately 1/3 seconds, it is related to maintaining of synchronism [24]. The second stage comes directly after the electromagnetic release; it lasts in range of few seconds and it is known as the IR. In terms of rotor angle stability, the IR in the grid is connected to a change of the rotor angle of synchronous machines. Sufficient amount of grid inertia supports to keep this angle within certain bounds to remain synchronism. In terms of frequency stability, it influences the rate of change of frequency (ROCOF), which is an important parameter for activating protective relays; and the maximal deviation of frequency, which is directly connected to load shedding [21], [23].

The third stage is the activation of PFR, which should start within a few seconds, and be fully deployed by 30 s. PFR stabilizes frequency in steady state with constant deviation from the nominal frequency. The subsequent action is deployment of secondary control reserve within 15 minutes to bring frequency to the nominal value and free up the PFR. Further it is followed and supported by tertiary control reserve, which frees up the previous reserves [25].

In the context of synchronous machines, the IR is understood as the inherent release of the stored kinetic energy in the rotating generator's rotor whenever there is an unbalance between generation and demand. In this case, the stored energy (E_{stored}) of a synchronous generator is determined by rotor moment of inertia (J) and its rotational speed (ω), as shown below [23],

$$E_{stored} = \frac{1}{2} J\omega^2. \tag{1}$$

When there is an unbalance of generation (P_{gen}) and demand (P_{load}) in the active power of the system with power rating S_{rated}, the ROCOF is given by the swing equation [27],

$$\frac{2H}{\omega}\frac{d\omega}{dt} = \frac{P_{gen} - P_{load}}{S_{rated}} = \frac{\Delta P}{S_{rated}} \tag{2}$$

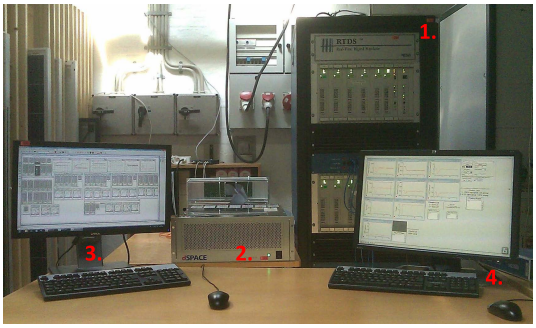


Fig. 2. Photo of the laboratory setup: 1. RTDS, 2. dSPACE, 3. Computer with RSCAD (RTDS simulation control) and 4. Computer with ControlDesk (dSPACE simulation control).

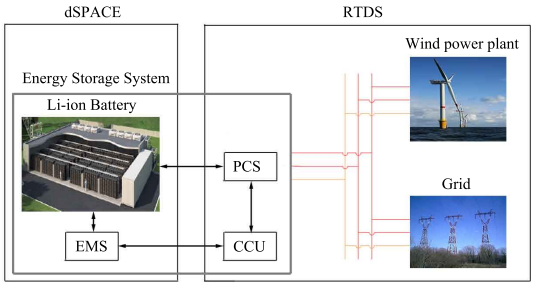


Fig. 3. Model layout composition with represented distribution to simulation platforms.

where, H is the inertia constant defined in [27] as

$$H = \frac{E_{stored}}{S_{rated}} = \frac{1}{2}\frac{J\omega^2}{S_{rated}}. \tag{3}$$

The typical value of the inertia constant for the CPP is between 2-9 seconds [28].

For the whole system, inertia constant can be calculated by,

$$H_{sys} = \frac{\sum_{i=1}^{n} H_i S_i}{S_{sys}} \tag{4}$$

where, H_i is inertia constant of the i-th unit, S_i is power rating of the i-th unit, H_{sys} is inertia constant of the system and S_{sys} is power rating of the system.

III. Simulation Environment

For investigating the technical viability of providing IR with Lithium-ion battery ESS, a setup consisting of two real-time simulators (i.e. RTDS and dSPACE) was built. The laboratory setup is shown in Fig. 2. The 12-bus grid model is simulated in RTDS and it is externally connected to the battery simulator and its energy management system (EMS). With this setup, it is possible to test the developed controller with a realistic battery model. Further, a physical battery may be connected to the simulator through an amplifier. The actual model layout composition is shown in Fig. 3.

A. Grid Model

The grid (see Fig. 4) was modelled in RSCAD. It is based on the generic 12-bus system model for wind power integration studies described in [29]. Wind power plants are modelled as inverters with a dc power source to represent the wind power generation, as depicted in Fig. 5. They do not provide any inertial or frequency response. The rating of every single WPP is 220 MVA.

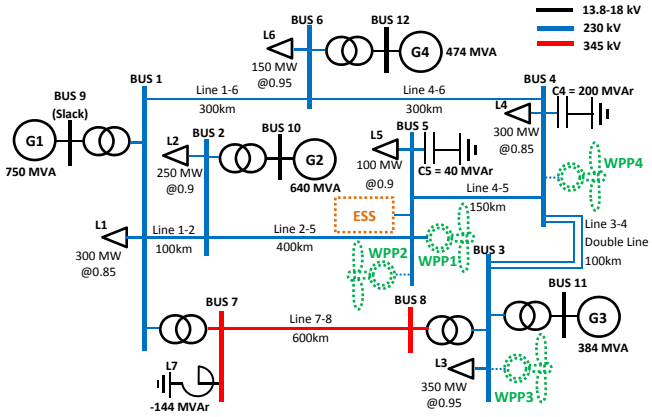


Fig. 4. 12-bus grid model.

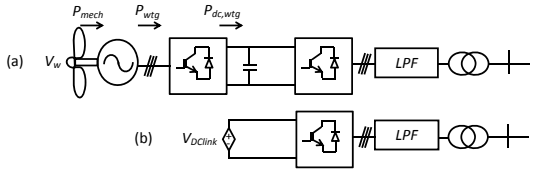


Fig. 5. a) Topology of wind turbine generator with full scale converter and b) simplified used aggregated model.

B. Energy Storage System Model

Modelling of the ESS consists of four parts and the structure of the model is presented in Fig. 3. The Li-ion battery and EMS are modelled in Simulink and simulated in dSPACE. The power conditioning system (PCS) and converter control unit (CCU) are modelled in RSCAD and simulated in RTDS. The modelled PCS has the same structure as it is shown in Fig. 5 b), with the difference that the voltage of the voltage source is determined by the terminal voltage of the detailed battery model desribed later.

1) Battery Model: As a simplification, it was considered that all the batteries were connected in series. In order to obtain the desired power rating, a battery scale factor is used in the RTDS model to reach the desired power rating. It was assumed that batteries are kept in air conditioned environment at 25 °C. Consequently, thermal influence on the batteries' performance is neglected. The Li-ion battery model was modelled based on the equivalent electrical circuit (EEC) from dSPACE Automotive Simulation Models library [20], which was proposed and validated by Chen and Mora in [19]. This detailed model is applied in order to represent Li-ion battery dynamics during IR. This dynamics influence battery operation in terms of output power, charging/discharging capability and safety limits. To describe the battery dynamics, internal resistance (R_{Bat}), inductance (L_{Bat}), double layer behavior (C_{DL}, R_{DL}) and diffusion behavior (C_{diff}, R_{diff}) are considered. A typical voltage profile obtained for a discharging current pulse is presented in Fig. 7. Moreover, the connection between the elements of the EEC and phenomenon which are occurring with different time constants are highlighted as well in Fig. 7. The use of a more simplified model without considering the dynamics would not provide accurate behavior in the observed short time period.

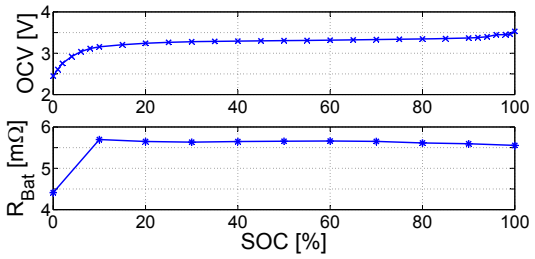


Fig. 6. Variation of open-circuit voltage (OCV) and internal resistance (R_{Bat}) versus the SOC of the $LiFePO_4$/C Li-ion battery.

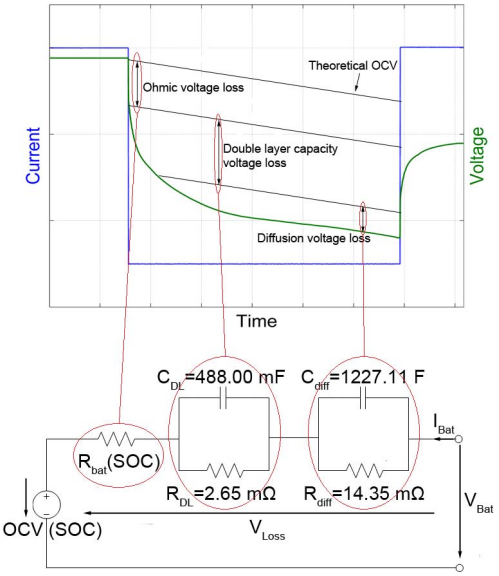


Fig. 7. The typical Li-ion battery voltage drop profile under the constant current discharge with assigned dynamics parts to the elements of the used EEC.

For parameterization of the Li-ion battery model, the chemistry with Lithium Iron Phosphate cathod and Graphite anode, $LiFePO_4$/C was considered. The battery model parameters were obtained from experimental measurements and from manufacturer data sheets [30], [31]; the nominal power of the battery cell was considered at the nominal voltage and a current of 10 A. The cell open circuit voltage (OCV) is dependant on the SOC and its profile is shown in Fig. 6. The other parameters of the EEC are derived from electrochemical impedance spectroscopy measurements, described in detail in [32]. The dependence of the internal resistance (R_{Bat}) on SOC is presented in Fig. 6. Finally, the EEC layout with the constant element parameters assigned to battery dynamics parts is shown in Fig. 7. The non-linear dependancy of the battery model parameters on current rate was not taken into account.

2) Energy Management System: The EMS controls the IR based on derivative control and on battery cells safety limits. The EMS scheme is shown in Fig. 8. The input is the frequency measurement. The parameters are asssumed as $K = 10$, which stands for providing nominal power from the ESS, when ROCOF is 0.1 Hz/s and higher; and $T = 1$, which is based on results from performed simulations with varying T. A ROCOF deadzone is considered in the range of ± 0.001 Hz/s that the ESS does not react to very small fluctuations. A factor of 5000 is used to convert the power

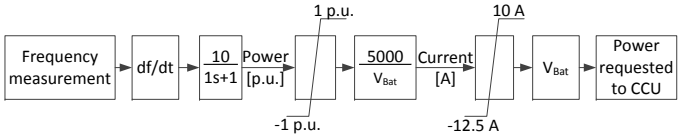


Fig. 8. The EMS block diagram.

from per unit system to absolute value. Limitations for current and voltage are applied based on [30], [31]. The safety control acts and disable providing of the IR, when the cell voltage is below 2 V and above 4 V and when the SOC reaches 0 % or 100 %. The power requested is computed and sent to the CCU. The real power processed by the ESS into the grid is measured and applied back to the battery model. For the operation, the initial SOC level is set at 50 %. Thus, the ESS is capable to respond to frequency deviations in both directions.

IV. Study Cases

The objectives of the study were to investigate the changes in IR due to RES grid integration and afterwards improve the response by utilizing ESSs. The study cases have been carried out considering the methodology for assessment of IR proposed in [22]. At the beginning of simulation, the system is in steady state. The observing time period is ten seconds. The CPP G2 consists of four generation units. The frequency dynamics of the system is studied in the event of tripping of two units of G2, which results in an immediate loss of 200 MW at t = 1.0 s. The operational metric focuses on the minimum point of the frequency (f_{min}) and ROCOF. In [25], the instantaneous minimum acceptable point of the frequency after loss of generation is determined as 49.2 Hz for grids operating at 50 Hz. According to [22], the maximal acceptable value of ROCOF is considered as 0.4 Hz/s. The ROCOF is computed from frequencies at time 1.0 s and 1.5 s, which covers 500 ms detection time of relays. The frequency is monitored at Bus 5 as the bus with the highest WPP penetration and connection of the ESS. Frequencies at other buses vary based on distances and generator swinging; the maximum frequency deviation among different busses was found to be 0.05 Hz by simulation.

Two study cases have been performed. The first study case analyzes different levels of wind power penetration in the grid and describes their impact in terms of IR. For the second study case, the ESS is connected into the grid. Scenarios with different ESS sizes, in terms of nominal power, are presented and the utilisation of the ESS based on Li-ion batteries is evaluated. Furthermore, the second study case answers the question, what ESS size is necessary to eliminate the effect of the RES integration towards IR in the studied system.

A. Study Case I.

This study case analyzes the effects of increasing wind power penetration in the grid on the IR. Five scenarios with different wind power penetration levels have been considered. The first scenario without any wind power penetration represents the original 12-bus system. Scenarios with 9 % and 16 % follow a pattern, where the load is increased with increasing the wind power penetration. The scenarios with 24 % and 33 % wind power penetration follow the second pattern, where increasing the wind power penetration causes decrease of CPPs. With each step of increasing wind power penetration level in the grid, one additional WPP is connected. Power production of the WPPs is assumed constant at all time. For the scenarios with 16, 24 and 33 % wind power penetration, the capacitor bank C5 is increased to 60 MVAr. In the case of 24 % wind power penetration, one generation unit of the CPP G3 (192 MVA) is switched off. Furthermore, with 33 % wind power penetration, two units of CPP G1 (in total 250 MVA) are additionaly disconnected. The list of scenarios and summary of the steady state active power parameters for CPPs, loads, and WPPs are summarized in Table I.

TABLE I
THE PARAMETERS FOR THE 12-BUS SYSTEM IN STEADY STATE, INCLUDING SYSTEM LOSSES.

Study Case I. - Scenario	1	2	3	4	5
Wind power penetration	0 %	9 %	16 %	24 %	33 %
CPP [MW]	1478	1473	1468	1265	1060
Load [MW]	1450	1650	1850	1850	1850
WPP [MW]	0	200	400	600	800
Total system rating [MVA]	2248	2468	2688	2716	2686

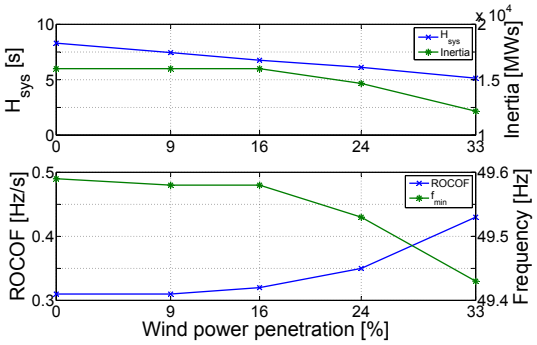


Fig. 9. Study Case I.: Overall inertia in the system and H_{sys} in upper plot; ROCOF and minimum frequency in lower plot.

The inertia over the system and system inertia constant (H_{sys}) are shown in Fig. 9. H_{sys} is computed theoretically according to (4) from the generator parameters considering the situation after tripping two units from G2. Fig. 9 reflects the applied two patterns in increasing wind power penetration. In the first pattern, even though the total system inertia in absolute values remains unchanged, the per unit system inertia equivalent decreases due to increasing system size. In the second pattern - reducing CPPs, the total system inertia decreases as well.

The effects of wind power penetration levels on the ROCOF and f_{min} are shown in Fig. 9. With the first pattern, the ROCOF is increased about 0.01 Hz/s and f_{min} is decreased about 0.01 Hz from the original scenario. It can be evaluated that the grid IR is intact and there is no impact to the grid stability.

In the scenarios following the second pattern, 24 % and 33 % wind power penetration, ROCOF is increased about 0.04 and 0.12 Hz/s and f_{min} is decreased about 0.06 and 0.16 Hz, respectively. Even the scenario with the highest 33 % wind power penetration (f_{min} = 49.43 Hz) fullfils the requirement of f_{min} above the acceptable value of 49.2 Hz. However,

TABLE II
THE RESULTS FOR STUDY CASE I.

Wind power penetration	ROCOF [Hz/s]	f_{min} [Hz]	H_{Bus5} [s]	H_{sys} [s]
0 %	0.31	49.59	8.25	8.30
9 %	0.31	49.58	7.47	7.45
16 %	0.32	49.58	6.50	6.76
24 %	0.35	49.53	5.97	6.12
33 %	0.43	49.43	4.88	5.14

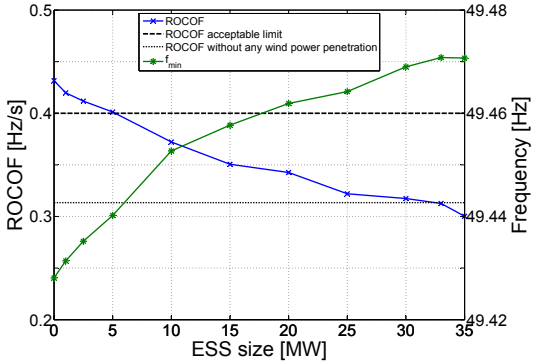


Fig. 10. Study Case II.: ROCOF and f_{min} with different ESS sizes.

maximal ROCOF limit 0.4 Hz/s is violated in the scenario with 33 % wind power penetration. The second pattern, reducing of CPPs, has visible impact to the grid IR and the grid stability is endangered.

The numerical results of ROCOF, f_{min}, H_{Bus5} and H_{sys} are presented in Table II. The inertia constant H_{Bus5} is computed according to (2) from measurements at Bus 5. H_{sys} is computed from the set parameters of generation units. H_{sys} and H_{Bus5} differ from each other in the interval of $[-0.2, 0.26]$ s.

The increase of wind power penetration in the grid results in decrease of the IR. This further results in increasing ROCOF and decreasing minimal point of frequency after the sudden disturbance, as it can be a generation loss or switching on a load.

B. Study Case II.

Due to negative effects of RES grid integration on the ROCOF and minimal point of frequency, the ESS based on Li-ion batteries is used to provide IR to the grid. In this context, it is evaluated the contribution to the grid IR and the influence of the ESS size.

To carry out this study, the ESS is connected to Bus 5, as shown in Fig. 4. The nominal power of the ESS is varied from 1 MW to 35 MW. The results for ROCOF and f_{min} are presented in Fig. 10 and Table III. Because f_{min} has not violated the limit of acceptable minimum frequency in the scenario without the ESS, it is not of any concern here. ROCOF violates the acceptable limits, unless an ESS with nominal power higher than 5 MW is not connected.

For the studied conditions, in order to provide the same IR in terms of ROCOF as in the scenario without any wind power penetration level, the necessary size of the ESS is found to be 33 MW. This represents 7.47 % of reduced CPP nominal power in the system and 3.75 % of the total installed wind

TABLE III
THE RESULTS FOR STUDY CASE II.

ESS nominal power [MW]	ROCOF [Hz/s]	f_{min} [Hz]	H_{Bus5} [s]	H_{sys} [s]
0	0.43	49.43	4.88	5.14
1	0.42	49.43	5.01	5.16
2.5	0.41	49.44	5.11	5.20
5	0.40	49.44	5.25	5.26
10	0.37	49.45	5.66	5.40
15	0.35	49.46	6.01	5.55
20	0.34	49.46	6.15	5.69
25	0.32	49.46	6.54	5.86
30	0.32	49.47	6.64	5.99
33	0.31	49.47	6.78	6.08
35	0.30	49.47	7.02	6.15

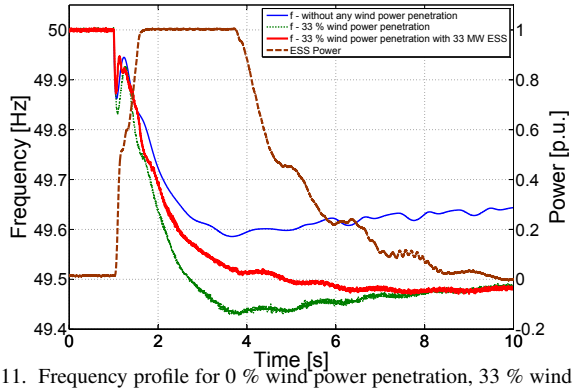


Fig. 11. Frequency profile for 0 % wind power penetration, 33 % wind power penetration and 33 % wind power penetration with the 33 MW ESS, together with the power provided by this ESS.

power capacity. In Fig. 11, there is shown a comparison of frequency profiles for the scenarios without the ESS with 0 % and 33 % wind power penetration and the scenario with the 33 MW ESS with 33 % wind power penetration. The minimal frequency and the steady state frequency values are as well dependant on the PFR. Utilisation of the ESS in this case reduces the typical valley with the frequency nadir. Due to the reduced grid capability of the PFR by reducing CPPs, the steady state value of frequency is the same for the scenarios with 33 % wind power penetration with and without the ESS.

Expressing the inertia constant of the ESS (H_{ESS}) is not straightforward as is in the case of synchronous machines. By using (3), H_{ESS} is equal to 450 s. This value does not reflect the real contribution of the ESS to the IR in the grid. Therefore, (3) is not applicable in the case of the ESS. In order to estimate the H_{ESS}, the following approach has been chosen. In (2), ΔP is the measured power provided by the ESS, S_{rated} is the power rating of the ESS, ω and $\frac{d\omega}{dt}$ are measured values, all variables are related to t = 1.5 s. Finally, the average computed H_{ESS} is 62.69 s, which is still not comparable to CPP values. The H_{sys} is subsequently computed from (4) including the ESS unit (individual H_{ESS} and S_{ESS}) and it is evaluated as the overall system inertia constant. Directly from (2) and frequency measurements at Bus 5, H_{Bus5} is computed and it represents inertia constant for the system appearing at Bus 5. H_{sys} and H_{Bus5} show the contribution of the ESS towards IR in the system and its placement in Table III.

From the ESS point of view, providing IR with the applied settings causes in average only 0.5 % decrease in the SOC over the period of 10 s. This represents an inefficient utilization of the energy capacity, if the ESS provides only IR.

V. Conclusion

With RES grid integration resulting in reducing the number of CPPs, the grid IR is decreased and it can result in endangering the grid stability. Real time simulations for five different scenarios were performed to analyze the effect of wind power penetration in the studied system. It was observed that 33 % wind power penetration caused 0.12 Hz/s increment in ROCOF and 0.16 Hz decrement in the minimum frequency. The measured minimum frequency 49.43 Hz is higher than the least acceptable value of 49.2 Hz, but the ROCOF exceeds the allowed limits by 0.03 Hz/s.

The utilisation of the ESS has shown that the impact of wind power penetration on the IR can be reduced or neutralised with an appropriate size of the ESS. For the considered 33 % wind power penetration level, at least a 5 MW ESS is necessary to bring the ROCOF back to acceptable limit of 0.4 Hz/s. A large ESS is necessary for providing the similar grid IR as it is in the grid without any wind power penetration. It was found to be 33 MW Li-ion ESS for 2686 MVA test system. The effectivity of usage the ESS energy capacity is very low. Therefore the utilization of Li-ion ESS only for providing IR might be not suitable from the economic point of view.

Providing IR in combination with an other grid service, such as primary frequency regulation, can improve both the usage of the ESS capacity and the steady state value of the frequency. The overall performance of the ESS can be as well improved by combining the Li-ion battery technology with the supercapacitor ES technology into a hybrid system.

References

[1] (2009, April) Directive 2009/28/EC of the European Parliament and of the Council of 23 April 2009 on the promotion of the use of energy from renewable sources and amending and subsequently repealing Directives 2001/77/EC and 2003/30/EC (Text with EEA relevance). Directive. European Parliament, Council.

[2] "Energy policy report 2012," Ministry of Climate, Energy and Building, Denmark, Tech. Rep., May 2012.

[3] "National Electricity Transmission System Seven Year Statement," National Grid UK, Tech. Rep., May 2011.

[4] P. Tielens and D. V. Hertem, "Grid Inertia and Frequency Control in Power Systems with High Penetration of Renewables," in *Young Researchers Symposium in Electrical Power Engineering*, vol. 6, Delft, The Netherlands, April 2012.

[5] J. Zhu, C. Booth, G. Adam, A. Roscoe, and C. Bright, "Inertia emulation control strategy for vsc-hvdc transmission systems," *Power Systems, IEEE Transactions on*, vol. 28, no. 2, pp. 1277–1287, May 2013.

[6] P. W. Christensen and G. C. Tarnowski, "Inertia for Wind Power Plants - state of the art review - year 2011," in *10th International Workshop on Large-Scale Integration of Wind Power into Power Systems*, Aarhus, Denmark, October 2011.

[7] N. Miller and P. Marken, "Facts on grid friendly wind plants," in *Power and Energy Society General Meeting, 2010 IEEE*, 2010, pp. 1–7.

[8] W. Gu, W. Liu, C. Shen, and Z. Wu, "Multi-stage underfrequency load shedding for islanded microgrid with equivalent inertia constant analysis," *International Journal of Electrical Power & Energy Systems*, vol. 46, pp. 36 – 39, 2013.

[9] M. Benidris and J. Mitra, "Enhancing stability performance of renewable energy generators by utilizing virtual inertia," in *Power and Energy Society General Meeting, 2012 IEEE*, 2012, pp. 1–6.

[10] G. Delille, B. Francois, and G. Malarange, "Dynamic Frequency Control Support by Energy Storage to Reduce the Impact of Wind and Solar Generation on Isolated Power System's Inertia," *Sustainable Energy, IEEE Transactions on*, vol. 3, no. 4, pp. 931–939, 2012.

[11] M. ud din Mufti, S. A. Lone, S. J. Iqbal, M. Ahmad, and M. Ismail, "Super-capacitor based energy storage system for improved load frequency control," *Electric Power Systems Research*, vol. 79, no. 1, pp. 226 – 233, 2009.

[12] S. Padrn, J. Medina, and A. Rodrguez, "Analysis of a pumped storage system to increase the penetration level of renewable energy in isolated power systems. gran canaria: A case study," *Energy*, vol. 36, no. 12, pp. 6753 – 6762, 2011.

[13] A. Tuohy and M. OMalley, "Pumped storage in systems with very high wind penetration," *Energy Policy*, vol. 39, no. 4, pp. 1965 – 1974, 2011.

[14] J. Zhang, "Research on Flywheel Energy Storage System Using in Power Network," in *Power Electronics and Drives Systems, 2005. PEDS 2005. International Conference on*, vol. 2, 2005, pp. 1344–1347.

[15] M. Albu, A. Nechifor, and D. Creanga, "Smart storage for active distribution networks estimation and measurement solutions," in *Instrumentation and Measurement Technology Conference (I2MTC), 2010 IEEE*, 2010, pp. 1486–1491.

[16] M. Datta, H. Ishikawa, H. Naitoh, and T. Senjyu, "LFC by coordinated virtual inertia mimicking and PEVs in power utility with MW-class distributed PV generation," in *Control and Modeling for Power Electronics (COMPEL), 2012 IEEE 13th Workshop on*, 2012, pp. 1–8.

[17] F. Daz-Gonzlez, A. Sumper, O. Gomis-Bellmunt, and R. Villaffila-Robles, "A review of energy storage technologies for wind power applications," *Renewable and Sustainable Energy Reviews*, vol. 16, no. 4, pp. 2154 – 2171, 2012.

[18] M. Swierczynski, D. Stroe, A.-I. Stan, R. Teodorescu, and S. J. Andreasen, *Evaluation of Different Operational Strategies for Lithium Ion Battery Systems Connected to a Wind Turbine for Primary Frequency Regulation and Wind Power Forecast Accuracy Improvement*. Energynautics GmbH, 2012.

[19] M. Chen and G. Rincon-Mora, "Accurate electrical battery model capable of predicting runtime and i-v performance," *Energy Conversion, IEEE Transactions on*, vol. 21, no. 2, pp. 504–511, June 2006.

[20] "dSPACE HelpDesk," [manual], November 2011, dSPACE GmbH.

[21] P. Kundur, J. Paserba, V. Ajjarapu, G. Andersson, A. Bose, C. Canizares, N. Hatziargyriou, D. Hill, A. Stankovic, C. Taylor, T. Van Cutsem, and V. Vittal, "Definition and classification of power system stability ieee/cigre joint task force on stability terms and definitions," *Power Systems, IEEE Transactions on*, vol. 19, no. 3, pp. 1387–1401, 2004.

[22] M. Altin, R. Teodorescu, B. Bak-Jensen, U. Annakkage, F. Iov, and P. Kjær, *Methodology for Assessment of Inertial Response from Wind Power Plants*, ser. IEEE Power and Energy Society General Meeting. IEEE Press, 2012, pp. 1–8.

[23] P. Kundur, N. Balu, and M. Lauby, *Power System Stability and Control*. McGraw-Hill Education, 1994.

[24] J. Machowski, J. Bialek, and J. Bumby, *Power System Dynamics: Stability and Control*. Wiley, 2008.

[25] "UCTE Operation Handbook," Union for the Co-ordination of Transmission of Electricity, Tech. Rep., 2004.

[26] A. Oudalov, D. Chartouni, and C. Ohler, "Optimizing a Battery Energy Storage System for Primary Frequency Control," *Power Systems, IEEE Transactions on*, vol. 22, no. 3, pp. 1259–1266, Aug.

[27] I. J. Nagrath and D. P. Kothari, *Power System Engineering*. Tata McGraw-Hill, 2007, iSBN 9780070647916.

[28] J. Morren, J. Pierik, and S. W. de Haan, "Inertial response of variable speed wind turbines," *Electric Power Systems Research*, vol. 76, no. 11, pp. 980 – 987, 2006.

[29] A. Adamczyk, M. Altin, Ömer Göksu, R. Teodorescu, and F. Iov, *Generic 12-Bus Test System for Wind Power Integration Studies*. EPE Association, 2012.

[30] "A123 ALM12V7 Charging Considerations," [application note], A123 Systems, Inc., September 2012, a123 Systems, Inc.

[31] "Nanophosphate® High Power Lithium Ion Cell ANR26650M1-B," [data sheet], A123 Systems, Inc., 2012, a123 Systems, Inc.

[32] V. Knap and R. Sinha, "Grid Inertial Response with Lithium-ion Battery Energy Storage Systems," Master's thesis, Aalborg University, Denmark, 2013.